Rigorous Quasi-TEM Analysis of Multiconductor Transmission Lines in Bi-Isotropic Media—Part II: Numerical Solution for Layered Media

Frank Olyslager, *Member, IEEE*, Eric Laermans, and Daniël De Zutter, *Member, IEEE*

***Abstract*—An integral equation technique is used to determine the circuit parameters of the nonreciprocal and nonsymmetrical set of transmission lines that describe a multiconductor line in a layered bi-isotropic background in the quasi-TEM approximation. The integral equation is solved with the method of moments and pointmatching technique. The integrations arising in the problem are handled carefully to allow a fast and accurate implementation. The conductors have an arbitrary cross-section consisting of straight and circularly curved segments. At the edges of the conductors the singular behavior of the surface charge density and surface current density is explicitly taken into account.**

I. Introduction

In THIS paper the general potential problem of [1] is numerically solved for the important special case of multiconductor lines embedded in layered media. Hence, we will not repeat the whole introduction of [1] here, but we will concentrate on the numerical solution technique. Multiconductor lines with general cross-section embedded in layered bianisotropic media have been studied in the past in the full-wave regime [2] with the method of moments. In [3] the theory for a finite element method in general three-dimensional objects was developped. This theory could also be used for waveguide problems. The publication [3] was, however, restricted to the theory without numerical examples, and for open structures it has been shown in the past that an integral equation technique is more suited. In the present contribution we concentrate on a quasi-TEM analysis for multiconductor lines with a cross-section consisting of straight and circularly curved segments. A quasi-TEM analysis has the advantage to be much faster than a full-wave analysis and, for example, for printed circuit boards and many MMIC applications a quasi-TEM analysis is often satisfactory.

In the past, it has been shown that the use of integral equation techniques is very adequate to solve two-dimensional potential problems of infinite extent, as has been shown in [4]–[7] for general cross-section multiconductor lines in isotropic layered media and in [8] for thin strips in layered media. In the present paper we will generalize the, in our opinion, very efficient technique of [7] to bi-isotropic layered media. We want to remark that although we assume bi-isotropic materials, the present method can also be used for certain bianisotropic materials as has been discussed in [1].

The method in [7] is a space domain method of moments and pointmatching technique. The layered medium in [7] is taken care of by using the Green's function of the layered medium. The speed and accuracy of the method is a consequence of the fact that the dependency of the excitation and observation point in the spectral Green's function is known under analytical form and the fact that the singular behavior at the edges of the conductors is taken into account. Fortunately, much of the numerical technique, especially the spectral and basis function integrations, does not change when generalizing [7] to bi-isotropic layers. This allows us to mainly restrict ourselves in this paper to two things that are fundamentally different for the bi-isotropic case. The first one is the calculation of the spectral Green's function, which is much more complicated than in [7] and second the singular behavior at edges. For this singular behavior we use the results of [9]. Another difference from [7] is, of course, that the electric and magnetic problem have to be solved simultaneously. In the paper we try to give a full, detailed description of the solution technique, however without becoming redundant, i.e. without repeating most of the details already put forward in [7].

Aside from the theory, a number of numerical examples are included to illustrate the generality of the approach and to illustrate the properties of the bitransmission line parameters $\overline{\overline{C}}, \overline{\overline{L}}, \overline{\overline{X}}$, and $\overline{\overline{Z}}$ derived in [1]. The examples are also compared with results obtained in [10]. In [10] a quasi-static image method was used to analyse a single thin microstrip on a bi-isotropic substrate. The emphasis of this paper was on the image technique and a very simple numerical technique was used to solve the problem. A discrepancy between our results and the results in [10] for the impedance of the microstrip line is explained.

II. Outline of the Solution

Consider the structure of Fig. 1 with L lossless bi-isotropic layers. Layer i $(i = 1, 2, \cdots, N)$ has thickness d_i and material parameters $\varepsilon_i, \mu_i, \zeta_i$ and ξ_i. At the top and bottom of the structure there is either a semi-infinite layer or a perfectly conducting ground plane. For a semi-infinite layer at the bottom (top) of the structure we set d_1 (d_L) equal to zero.

Manuscript received September 27, 1994; revised December 14, 1994. This work was supported by the Belgian National Fund of Scientific Research (NFWO).

The authors are with the Electromagnetics Group, Department of Information Technology, University of Ghent, 9000 Ghent, Belgium.

IEEE Log Number 9412055.

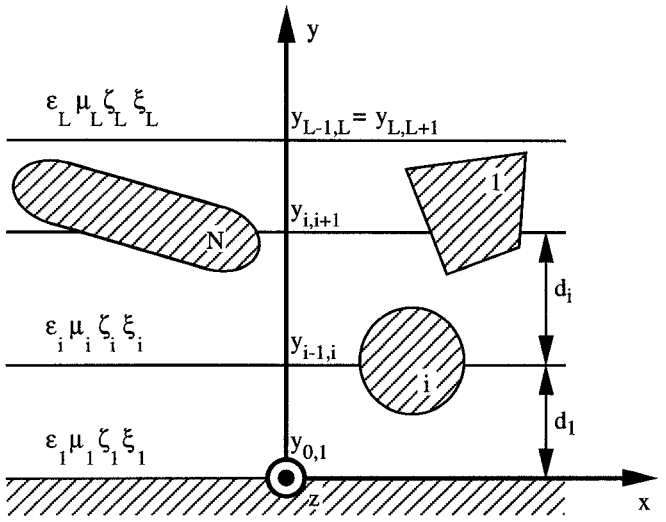

Fig. 1. Geometry of a multiconductor line in a layered bi-isotropic background medium.

Quantities defined at the interface between two layers are indicated by a double subscript. For example $y_{i-1,i}$ is the y-coordinate of the interface between layer $i-1$ and layer i. The y-coordinate at the bottom (top) of the structure is denoted by $y_{0,1}$ ($y_{L,L+1}$). N perfect electrical conducting (PEC) conductors are embedded in the planar stratified medium. It is assumed that no conductors are embedded in semi-infinite layers. This is no restriction because one can always insert a fictitious layer interface. The cross-section of each conductor is bounded by straight or circularly curved segments. The boundary curve of conductor k is denoted by c_k. For the other notations we refer the reader to [1].

Due to the layered nature of the structure, the potential problem defined in [1] simplifies drastically. In each layer the potentials ϕ and ψ now satisfy the ordinary simple Laplace equations $\nabla^2_{\rm tr}\phi = 0$ and $\nabla^2_{\rm tr}\psi = 0$. These two independent Laplace equations are coupled at the layer interfaces through the boundary conditions. At the interface between layer i and layer $i+1$ the boundary conditions are (with $n_i = \sqrt{\varepsilon_i \mu_i - \zeta_i \xi_i}$)

$$\begin{array}{cc} \phi \text{ continuous} & \psi \text{ continuous} \\ -\dfrac{n_i^2}{\mu_i}\dfrac{\partial \phi}{\partial y} - \dfrac{\xi_i}{\mu_i}\dfrac{\partial \psi}{\partial x} = -\dfrac{n_{i+1}^2}{\mu_{i+1}}\dfrac{\partial \phi}{\partial y} - \dfrac{\xi_{i+1}}{\mu_{i+1}}\dfrac{\partial \psi}{\partial x} & (1) \\ -\dfrac{\zeta_i}{\mu_i}\dfrac{\partial \phi}{\partial x} - \dfrac{1}{\mu_i}\dfrac{\partial \psi}{\partial y} = -\dfrac{\zeta_{i+1}}{\mu_{i+1}}\dfrac{\partial \phi}{\partial x} - \dfrac{1}{\mu_{i+1}}\dfrac{\partial \psi}{\partial y}. & \end{array}$$

The last two conditions express the continuity of $\boldsymbol{u}_y \cdot \boldsymbol{D}_{\rm tr,0}$ and $\boldsymbol{u}_y \times \boldsymbol{H}_{\rm tr,0}$.

From [1] it follows that the circuit matrices can be determined if one is able to find the surface charge density ρ_0 and surface current density $J_{z,0}$ on each conductor for a given distribution of the potentials ϕ_k and ψ_k ($k = 1, 2, \cdots, N$) of the conductors. We will solve this problem by means of a classical integral equation given by

$$\begin{pmatrix} \phi_k \\ \psi_k \end{pmatrix} = \lim_{r \to r_k} \sum_{j=1}^{N} \oint_{c_j} \begin{pmatrix} G_{\phi\rho}(\boldsymbol{r}|\boldsymbol{r}') & G_{\phi J}(\boldsymbol{r}|\boldsymbol{r}') \\ G_{\psi\rho}(\boldsymbol{r}|\boldsymbol{r}') & G_{\psi J}(\boldsymbol{r}|\boldsymbol{r}') \end{pmatrix} \cdot \begin{pmatrix} -\dfrac{\mu \rho_0(\boldsymbol{r}')}{n^2} \\ -\mu J_{z,0}(\boldsymbol{r}') \end{pmatrix} dc'$$
$$\forall k = 1, 2, \cdots, N \qquad \forall \boldsymbol{r}_k \in c_k. \qquad (2)$$

This is a coupled set of integral equations for the unknowns ρ_0 and $J_{z,0}$. The kernels of (2) are the Green's functions G_{ab} ($a = \phi$ or ψ and $b = \rho$ or J) of the layered medium. These Green's functions are solution of

$$\nabla^2_{\rm tr} \begin{pmatrix} G_{\phi\rho}(\boldsymbol{r}|\boldsymbol{r}') & G_{\phi J}(\boldsymbol{r}|\boldsymbol{r}') \\ G_{\psi\rho}(\boldsymbol{r}|\boldsymbol{r}') & G_{\psi J}(\boldsymbol{r}|\boldsymbol{r}') \end{pmatrix} = \delta(\boldsymbol{r} - \boldsymbol{r}') \begin{pmatrix} 1 & 0 \\ 0 & 1 \end{pmatrix} \qquad (3)$$

where $G_{\phi b}$ and $G_{\psi b}$ ($b = \rho$ or J) satisfy the boundary conditions (1) with ϕ, respectively ψ replaced by $G_{\phi b}$, respectively $G_{\psi b}$. In the sequel we will restrict ourselves to the calculation of $G_{\phi\rho}$ and $G_{\psi\rho}$ since the calculation of $G_{\phi J}$ and $G_{\psi J}$ is totally analogous.

These Green's functions are calculated in the classical way by using a spectral approach. By exploiting the symmetry of the spectral Green's functions we can write the relation between the spectral domain and space domain Green's functions, i.e. the inverse spatial Fourier transform, as

$$\begin{aligned} G_{\phi\rho}(\boldsymbol{r}|\boldsymbol{r}') &= \frac{1}{\pi} \int_0^{+\infty} G_{\phi\rho}(k_x, y|y') \cos\left[k_x(x - x')\right] dk_x \\ G_{\psi\rho}(\boldsymbol{r}|\boldsymbol{r}') &= -\frac{j}{\pi} \int_0^{+\infty} G_{\phi\rho}(k_x, y|y') \sin\left[k_x(x - x')\right] dk_x. \end{aligned} \qquad (4)$$

We introduce asymptotic and finite Green's functions $G^{as}_{a\rho}$ and $G^{fin}_{a\rho}$ ($a = \phi$ or ψ) as in [7]. $G^{as}_{a\rho}$ is calculated under the assumption that k_x is large allowing to express the k_x-dependence of $G^{as}_{a\rho}$ analytically. The function $G^{fin}_{a\rho}$ is taken equal to $G_{a\rho}$ when $k_x < k_c$ and equal to $G_{a\rho} - G^{as}_{a\rho}$ when $k_c < k_x < k_e$. At k_e the difference between $G_{a\rho}$ and $G^{as}_{a\rho}$ becomes negligible. For a discussion regarding the choice of k_c and k_e we refer to [7]. Taking into account these considerations we can rewrite the first equation of (4) as

$$\begin{aligned} G_{\phi\rho}(\boldsymbol{r}|\boldsymbol{r}') = \frac{1}{\pi} \int_0^{k_e} G^{fin}_{\phi\rho} \cos\left[k_x(x - x')\right] dk_x \\ + \frac{1}{\pi} \int_{k_c}^{+\infty} G^{as}_{\phi\rho} \cos\left[k_x(x - x')\right] dk_x \end{aligned} \qquad (5)$$

and similarly for $G_{\psi\rho}(\boldsymbol{r}|\boldsymbol{r}')$. Now we insert the expressions of type (5) in the integral equations (2) and interchange the finite integration $[0, k_e]$ with the integration over the contour c_j of each conductor as in [7].

As in [7] a method of moments technique combined with pointmatching is used to discretize the set of integral equations. For the division in segments of the contours c_k we refer to [7]. Within each segment we represent ρ_0 and $J_{z,0}$ as

$$\begin{aligned} \begin{Bmatrix} \rho_0(s) \\ J_{z,0}(s) \end{Bmatrix} &= s^{\nu_1 - 1} \begin{Bmatrix} 1 \\ \alpha_1 \end{Bmatrix} (A_0 + A_1 s) \\ &+ s^{\nu_2 - 1} \begin{Bmatrix} \alpha_2 \\ 1 \end{Bmatrix} (B_0 + B_1 s). \end{aligned} \qquad (6)$$

s is the distance from one of the endpoints of the considered segment. A_0, A_1 and B_0, B_1 are the unknowns for this segment and $\alpha_1, \nu_1, \alpha_2$, and ν_2 follow from the edge condition.

The singular behavior at an edge in bi-isotropic materials is discussed in [9]. The values of $\alpha_1, \nu_1, \alpha_2$, and ν_2 applicable in the case considered here are given in the Appendix. For a segment not containing an edge of the conductor $\alpha_1, \nu_1, \alpha_2$, and ν_2 are zero, which means that (6) is part of a Taylor series. If in this case we impose the continuity of (6) at the junction of two segments we obtain a piecewise linear representation for current and charge. By taking higher-order terms in s into account in (6), a piecewise parabolic or piecewise cubic representation can be obtained.

In the next sections we will show that the spectral Green's functions G_{ab}^{fin} ($a = \phi$ or ψ and $b = \rho$ or J) can be written in the same form as in [7] and that the asymptotic Green's functions G_{ab}^{as} also have the same k_x-dependence as in [7] (remark that k_y in [7] corresponds with k_x here). This means that the integrations over the basis functions and the evaluation of the spectral integrations are of the same type as in [7] and that we do not have to repeat these integrations here.

III. The Spectral Green's Function

In this section, the spectral Green's functions $G_{a\rho}(k_x, y|y')$ ($a = \phi$ or ψ) are calculated. We call y' the excitation point and y the observation point. y' is located in layer e and y is located in layer o, which eventually can coincide with layer e. In both these layers we introduce relative y-coordinates as $w_e = y' - y_{e-1,e}, v_e = y_{e,e+1} - y', w_o = y - y_{o-1,o}$, and $v_o = y_{o,o+1} - y$.

The Green's functions $G_{a\rho}(k_x, y|y')$ satisfy the following differential equations:

$$\frac{d^2G_{\phi\rho}}{dy^2} - k_x^2 G_{\phi\rho} = \delta(y - y') \quad \frac{d^2G_{\psi\rho}}{dy^2} - k_x^2 G_{\psi\rho} = 0 \tag{7}$$

with the following boundary conditions at the interface between layer i and $i+1$:

$$\begin{array}{cc} G_{\phi\rho}\text{ continuous} & G_{\psi\rho}\text{ continuous} \\ \dfrac{n_i^2}{\mu_i}\dfrac{dG_{\phi\rho}}{dy} - jk_x\dfrac{\xi_i}{\mu_i}G_{\psi\rho} = \dfrac{n_{i+1}^2}{\mu_{i+1}}\dfrac{dG_{\phi\rho}}{dy} - jk_x\dfrac{\xi_{i+1}}{\mu_{i+1}}G_{\psi\rho} & \\ -jk_x\dfrac{\zeta_i}{\mu_i}G_{\phi\rho} + \dfrac{1}{\mu_i}\dfrac{dG_{\psi\rho}}{dy} = -jk_x\dfrac{\zeta_{i+1}}{\mu_{i+1}}G_{\phi\rho} + \dfrac{1}{\mu_{i+1}}\dfrac{dG_{\psi\rho}}{dy} & \end{array} \tag{8}$$

This means that the column matrix $\boldsymbol{c}(y)$ defined as

$$\boldsymbol{c}(y) = \begin{pmatrix} G_{\phi\rho}(k_x, y|y') \\ \dfrac{n^2}{\mu}\dfrac{dG_{\phi\rho}(k_x, y|y')}{dy} - jk_x\dfrac{\xi}{\mu}G_{\psi\rho}(k_x, y|y') \\ G_{\psi\rho}(k_x, y|y') \\ -jk_x\dfrac{\zeta}{\mu}G_{\phi\rho}(k_x, y|y') + \dfrac{1}{\mu}\dfrac{dG_{\psi\rho}(k_x, y|y')}{dy} \end{pmatrix} \tag{9}$$

is continuous for all y-values except at the source level y'. The analytical solution of (7) in a layer $i \neq e$ allows us to calculate $\boldsymbol{c}_{i,i+1} = \boldsymbol{c}(y_{i,i+1})$ from $\boldsymbol{c}_{i-1,i} = \boldsymbol{c}(y_{i-1,i})$ as $\boldsymbol{c}_{i,i+1} = \exp(k_x d_i)\overline{\overline{N}}_i^u(d_i)\boldsymbol{c}_{i-1,i}$ with $\overline{\overline{N}}_i^u(\delta_y)$ given by (10), shown at the bottom of the page,
with $f^{\pm}(\delta_y) = 1 \pm \exp(-2k_x\delta_y)$. Note that this matrix does not contain any exponential functions with positive argument and is therefore suited for numerical implementation for large k_x-values. Similarly we can calculate $\boldsymbol{c}_{i-1,i}$ at the bottom of layer i from $\boldsymbol{c}_{i,i+1}$ at the top of this layer with $\boldsymbol{c}_{i-1,i} = \exp(k_x d_i)\overline{\overline{N}}_i^d(d_i)\boldsymbol{c}_{i,i+1}$ where $\overline{\overline{N}}_i^d(\delta_y)$ is equal to $\overline{\overline{N}}_i^u(\delta_y)$ in (10), shown at the bottom of the page, but with $f^{\pm}(\delta_y) = \exp(-2k_x\delta_y) \pm 1$. At the bottom and top of the structure we can write, respectively, $\boldsymbol{c}_{0,1}$ and $\boldsymbol{c}_{L,L+1}$ as

$$\begin{aligned} \boldsymbol{c}_{0,1} &= \overline{\overline{K}}^u \boldsymbol{R}^u \exp(-k_x w_e)\left[\prod_{i=1}^{e-1}\exp(-k_x d_i)\right] \\ \boldsymbol{c}_{L,L+1} &= \overline{\overline{K}}^d \boldsymbol{R}^d \exp(-k_x v_e)\left[\prod_{i=L}^{e+1}\exp(-k_x d_i)\right] \end{aligned} \tag{11}$$

with

$$\begin{aligned} \overline{\overline{K}}^u &= \begin{pmatrix} s & 0 \\ \dfrac{n_1^2}{\mu_1}k_x & -j\dfrac{\xi_1}{\mu_1}k_x \\ 0 & s \\ -j\dfrac{\zeta_1}{\mu_1}k_x & \dfrac{1}{\mu_1}k_x \end{pmatrix} \\ \overline{\overline{K}}^d &= \begin{pmatrix} -s & 0 \\ \dfrac{n_L^2}{\mu_L}k_x & j\dfrac{\xi_L}{\mu_L}k_x \\ 0 & -s \\ j\dfrac{\zeta_L}{\mu_L}k_x & \dfrac{1}{\mu_L}k_x \end{pmatrix} \end{aligned} \tag{12}$$

where $s = 0$ for a PEC plane and $s = 1$ for a semi-infinite layer. The two components of $\boldsymbol{R}^u$ and $\boldsymbol{R}^d$ are the four remaining unknowns of our problem which are determined by imposing the boundary conditions at the source level y'. As a last step we need the jump condition for $\boldsymbol{c}(y')$ at the source level y'

$$\boldsymbol{c}(y' + 0) - \boldsymbol{c}(y' - 0) = \begin{pmatrix} 0 \\ \dfrac{n_e^2}{\mu_e} \\ 0 \\ 0 \end{pmatrix}. \tag{13}$$

If we now express $\boldsymbol{c}(y' - 0)(\boldsymbol{c}(y' + 0))$ as a function of $\boldsymbol{c}_{0,1}(\boldsymbol{c}_{L,L+1})$ and use (11) and (13), we obtain the following

$$\overline{\overline{N}}_i^u(\delta_y) = \frac{1}{2}\begin{pmatrix} f^+(\delta_y) & \dfrac{\mu_i}{k_x n_i^2}f^-(\delta_y) & j\dfrac{\xi_i}{n_i^2}f^-(\delta_y) & 0 \\ k_x\varepsilon_i f^-(\delta_y) & f^+(\delta_y) & 0 & -j\xi_i f^-(\delta_y) \\ j\zeta_i f^-(\delta_y) & 0 & f^+(\delta_y) & \dfrac{\mu_i}{k_x}f^-(\delta_y) \\ 0 & -j\dfrac{\zeta_i}{n_i^2}f^-(\delta_y) & \dfrac{k_x\varepsilon_i}{n_i^2}f^-(\delta_y) & f^+(\delta_y) \end{pmatrix} \tag{10}$$

system of four linear equations for the four unknowns $\boldsymbol{R}^u$ and $\boldsymbol{R}^d$:

$$\overline{\overline{N}}_e^d(v_e)\overline{\overline{D}}_e\boldsymbol{R}^d - \overline{\overline{N}}_e^u(w_e)\overline{\overline{U}}_e\boldsymbol{R}^u = \begin{pmatrix} 0 \\ \dfrac{n_e^2}{\mu_e} \\ 0 \\ 0 \end{pmatrix} \tag{14}$$

with

$$\overline{\overline{D}}_i = \left[\prod_{j=L}^{i+1}\overline{\overline{N}}_j^d(d_j)\right]\boldsymbol{K}^d \quad \overline{\overline{U}}_i = \left[\prod_{j=1}^{i-1}\overline{\overline{N}}_j^u(d_j)\right]\boldsymbol{K}^u \tag{15}$$

and where the matrix products mean left multiplication. The solution of the system (14) is numerically easy but we need an analytical solution. After some very tedious calculations one finds that

$$\begin{pmatrix}\boldsymbol{R}^d \\ \boldsymbol{R}^u\end{pmatrix} = \begin{pmatrix}\boldsymbol{R}^{d(1)} \\ \boldsymbol{R}^{u(1)}\end{pmatrix} + \begin{pmatrix}\exp(-2k_x w_e)\boldsymbol{R}^{d(2)} \\ \exp(-2k_x v_e)\boldsymbol{R}^{u(2)}\end{pmatrix} \tag{16}$$

where $\boldsymbol{R}^{u(i)}$ and $\boldsymbol{R}^{d(i)}$ $(i = 1, 2)$ are given in the Appendix and are shown to be independent of the exact position of y' in the excitation layer, i.e. they are independent of v_e and w_e. With these expressions we can easily calculate $\boldsymbol{c}(y)$ at every position y. For example for an observation point y in a layer below the excitation layer we have

$$\begin{aligned}\boldsymbol{c}(y) = {} & \overline{\overline{N}}_o^u(w_o)\boldsymbol{U}_o\boldsymbol{R}^u \exp[-k_x(w_e + v_o)] \\ & \cdot \left[\prod_{i=o+1}^{e-1}\exp(-k_x\, d_i)\right].\end{aligned} \tag{17}$$

If $(o+1) > (e-1)$ the product at the end of (17) drops out and has to be replaced by one. Inserting (16) in (17) allows us to write the spectral Green's functions $G_{a\rho}(k_x, y|y')$ $(a = \phi$ or $\psi)$ as

$$\begin{aligned}G_{a\rho}(k_x, y|y') = {} & \{A_{a\rho}(k_x)\exp[-k_x(w_e + v_o)] \\ & + B_{a\rho}(k_x)\exp[-k_x(v_e + v_o + d_e)] \\ & + C_{a\rho}(k_x)\exp[-k_x(d_o + w_e + w_o)] \\ & + D_{a\rho}(k_x)\exp[-k_x(d_o + d_e + v_e + w_o)]\} \\ & \cdot \left[\prod_{i=o+1}^{e-1}\exp(-k_x\, d_i)\right]\end{aligned} \tag{18}$$

where the coefficients $A_{a\rho}(k_x), B_{a\rho}(k_x), C_{a\rho}(k_x)$, and $D_{a\rho}(k_x)$ are independent of w_e, v_e, w_o, and v_o. In other words, in (18) the dependence on the exact position of the excitation and observation level is known under full analytical form. The full expressions for $A_{a\rho}(k_x), B_{a\rho}(k_x), C_{a\rho}(k_x)$, and $D_{a\rho}(k_x)$ are given in the Appendix. Note that the expressions in (18) are indeed of the same form as the spectral Green's functions in [7]. The other cases where the observation is above the excitation level or where the excitation level is in the same layer as the observation layer are treated in a fully analogous way.

For large values of k_x a simplified solution of the layered medium is possible. In this case, as in [7], only four "waves" propagating from the excitation level y' to the observation level y are taken into account. For an interpretation of these four waves we refer to [7]. When the excitation layer is above the observation layer the asymptotic Green's functions $G_{a\rho}^{as}(k_x, y|y')$ are given by

$$\begin{aligned}\begin{pmatrix}G_{\phi\rho}(k_x, y|y') \\ G_{\psi\rho}(k_x, y|y')\end{pmatrix} = {} & -\frac{1}{2k_x}\{\overline{\overline{T}}\exp[-k_x(w_e + v_o)] \\ & + \overline{\overline{TK}}_{e,e+1}^u\exp[-k_x(v_e + v_o + d_e)] \\ & + \overline{\overline{K}}_{o-1,o}^d\overline{\overline{T}}\exp[-k_x(d_o + w_e + w_o)] \\ & + \overline{\overline{K}}_{o-1,o}^d\overline{\overline{TK}}_{e,e+1}^u\exp[-k_x(d_o + d_e \\ & + v_e + w_o)]\} \\ & \cdot \begin{pmatrix}1 \\ 0\end{pmatrix}\left[\prod_{i=o+1}^{e-1}\exp(-k_x\, d_i)\right]\end{aligned} \tag{19}$$

where

$$\overline{\overline{T}} = \prod_{i=e}^{o+1}\overline{\overline{T}}_{i-1,i}^d = \prod_{i=e}^{o+1}\left[\begin{pmatrix}1 & 0 \\ 0 & 1\end{pmatrix} + \overline{\overline{K}}_{i-1,i}^d\right] \tag{20}$$

and

$$\begin{aligned}\overline{\overline{K}}_{i,i+1}^u = {} & \frac{1}{\Delta_{i,i+1}}\begin{pmatrix} \dfrac{1}{\mu_i} + \dfrac{1}{\mu_{i+1}} & j\left(\dfrac{\xi_i}{\mu_i} - \dfrac{\xi_{i+1}}{\mu_{i+1}}\right) \\ j\left(\dfrac{\zeta_i}{\mu_i} - \dfrac{\zeta_{i+1}}{\mu_{i+1}}\right) & \dfrac{n_i^2}{\mu_i} + \dfrac{n_{i+1}^2}{\mu_{i+1}}\end{pmatrix} \\ & \cdot \begin{pmatrix} \dfrac{n_i^2}{\mu_i} - \dfrac{n_{i+1}^2}{\mu_{i+1}} & j\left(\dfrac{\xi_i}{\mu_i} - \dfrac{\xi_{i+1}}{\mu_{i+1}}\right) \\ j\left(\dfrac{\zeta_i}{\mu_i} - \dfrac{\zeta_{i+1}}{\mu_{i+1}}\right) & \dfrac{1}{\mu_i} - \dfrac{1}{\mu_{i+1}}\end{pmatrix} \\ \overline{\overline{K}}_{i-1,i}^d = {} & \frac{1}{\Delta_{i-1,i}}\begin{pmatrix} \dfrac{1}{\mu_{i-1}} + \dfrac{1}{\mu_i} & j\left(\dfrac{\xi_{i-1}}{\mu_{i-1}} - \dfrac{\xi_i}{\mu_i}\right) \\ j\left(\dfrac{\zeta_{i-1}}{\mu_{i-1}} - \dfrac{\zeta_i}{\mu_i}\right) & \dfrac{n_{i-1}^2}{\mu_{i-1}} + \dfrac{n_i^2}{\mu_i}\end{pmatrix} \\ & \cdot \begin{pmatrix} \dfrac{n_{i-1}^2}{\mu_{i-1}} - \dfrac{n_i^2}{\mu_i} & j\left(\dfrac{\xi_{i-1}}{\mu_{i-1}} - \dfrac{\xi_i}{\mu_i}\right) \\ j\left(\dfrac{\zeta_{i-1}}{\mu_{i-1}} - \dfrac{\zeta_i}{\mu_i}\right) & \dfrac{1}{\mu_{i-1}} - \dfrac{1}{\mu_i}\end{pmatrix}\end{aligned} \tag{21}$$

with

$$\Delta_{i,i+1} = \frac{(\varepsilon_i + \varepsilon_{i+1})(\mu_i + \mu_{i+1}) - (\xi_i + \xi_{i+1})(\zeta_i - \zeta_{i+1})}{\mu_i\mu_{i+1}} \tag{22}$$

$\overline{\overline{K}}^u$ and $\overline{\overline{K}}^d$ are reflection matrices and $\overline{\overline{T}}^d$ is a transmission matrix. If there is a ground plane at the bottom of the structure then $\overline{\overline{K}}_{0,1}^d$ is equal to minus the 2×2 unit matrix. Remark that (19) is of the same form as (18) with k_x-independent $A_{a\rho}, B_{a\rho}, C_{a\rho}$, and $D_{a\rho}$ coefficients except for the $1/2k_x$ factor in front of (19).

IV. Numerical Examples

In the first example we consider the microstrip structure of Fig. 2, which was also analyzed in [10]. The width w of the infinitely thin strip and the thickness d of the substrate are the same, i.e. $w = d$. The substrate consists of pure nonreciprocal bi-isotropic material with Tellegen parameter χ or pure reciprocal bi-isotropic material with chirality parameter

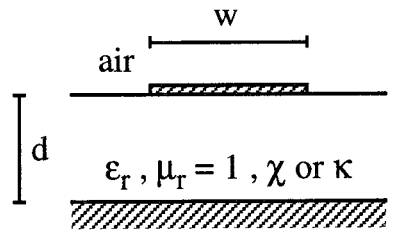

Fig. 2. Geometry of a microstrip on a bi-isotropic nonreciprocal or chiral substrate.

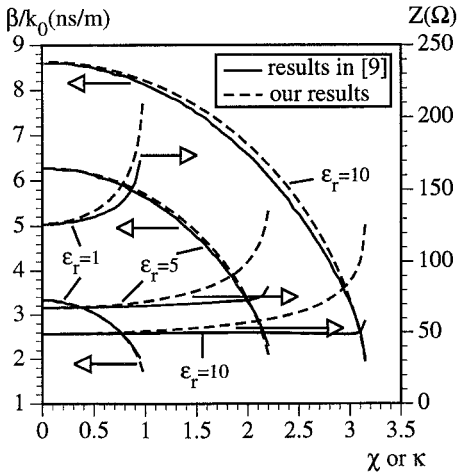

Fig. 3. Propagation coefficients $\beta\omega$ and impedances for the structure of Fig. 2, with $w = d$, as a function of the Tellegen parameter χ or the chirality parameter κ for $\varepsilon_r = 1, 5, 10$. The full lines are the solutions found in [9] and the dashed lines are our results.

κ. The substrate further has a relative dielectric constant ε_r. The graph on Fig. 3 shows a comparison of our results with the results obtained in [10]. Since the microstrip is a symmetrical structure we have that $X = Y = 0$. Due to the properties discussed in [1], the same results are obtained for a chiral substrate where κ is taken equal to χ. This means that the normalized propagation coefficient $\beta\omega$ and the impedance Z are given, respectively, by $\sqrt{LC}$ and $\sqrt{L/C}$. For our calculations we used 10 divisions on the strip. From the graph it is seen that there is a good agreement for $\beta\omega$ but that there is a considerable disagreement for Z for larger values of χ. We suspect that the difference is due to the fact that the full coupling between the electric and magnetic problem is not taken into account in [10]. In (60) of [10], it is assumed that the charge density (current density) does not generate magnetic flux (electric potential). This probably explains the difference in the results. The fact that the agreement for the propagation coefficients is better than the agreement for the impedance is not surprising since the propagation constant is always less susceptible to small inaccuracies. Errors of the same origin in C and L cancel out in the propagation constant and amplify each other in the impedance. Note further that the impedances become infinite for $\chi = \sqrt{\varepsilon_r}$ or $\kappa = \sqrt{\varepsilon_r}$, i.e. for $n = 0$.

As a second example we consider the structure of Fig. 4 consisting of four wires embedded in three bi-isotropic layers. The dimensions and material parameters are indicated on the figure. We used 24 divisions on each wire, which is more than

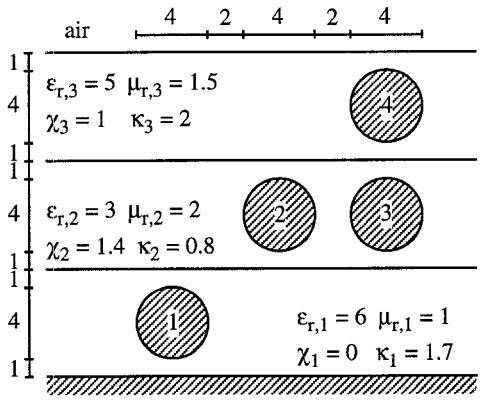

Fig. 4. Geometry of four identical wires embedded in a three-layered bi-isotriopic medium.

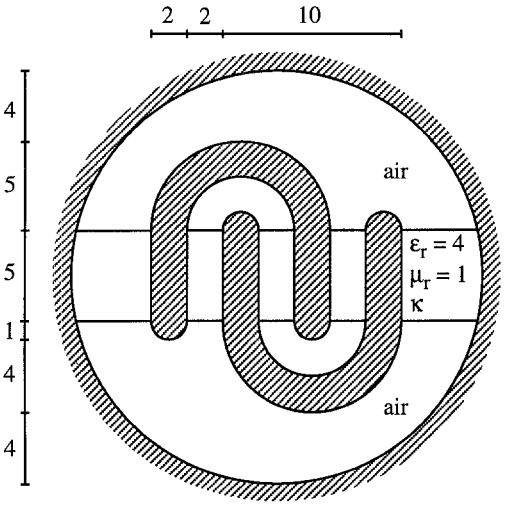

Fig. 5. Geometry of two horseshoe-shaped conductors in a layered bi-isotropic structure surrounded by a cylinder.

sufficient. With the numbering of the figure, the bitransmission line parameters are given by

$$\overline{\overline{C}} = \begin{pmatrix} 186.88 & -21.70 & -2.39 & -1.64 \\ -21.70 & 85.64 & -30.69 & -13.27 \\ -2.39 & -30.69 & 95.09 & -31.58 \\ -1.64 & -13.27 & -31.58 & 62.68 \end{pmatrix} \text{pF/m}$$

$$+ j \begin{pmatrix} 0.0 & 80.32 & -37.53 & -109.49 \\ -80.32 & 0.0 & 20.22 & 116.79 \\ 37.53 & -20.22 & 0.0 & 119.30 \\ 109.49 & -116.79 & -119.30 & 0.0 \end{pmatrix} \text{fF/m}$$

$$\overline{\overline{L}} = \begin{pmatrix} 194.20 & 64.88 & 36.06 & 33.37 \\ 64.88 & 551.86 & 243.23 & 212.81 \\ 36.06 & 243.23 & 552.07 & 284.30 \\ 33.37 & 212.81 & 284.30 & 607.90 \end{pmatrix} \text{nH/m}$$

$$+ j \begin{pmatrix} 0.0 & -10.18 & -144.34 & -342.28 \\ 10.18 & 0.0 & 348.15 & 1397.0 \\ 144.34 & -348.15 & 0.0 & 1145.4 \\ 342.28 & -1397.0 & -1145.4 & 0.0 \end{pmatrix} \text{pH/m}$$

$$\overline{\overline{X}} = \begin{pmatrix} -28.56 & 74.97 & 35.77 & -23.94 \\ -216.59 & -4.72 & 141.49 & -71.12 \\ -117.59 & -89.30 & 44.25 & 8.33 \\ -40.21 & 50.95 & -5.76 & -12.71 \end{pmatrix} \text{ps/m}$$

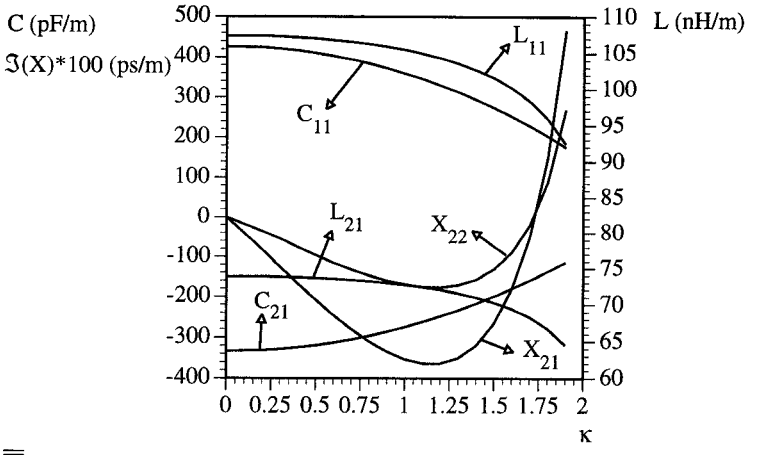

Fig. 6. The parameters $\overline{\overline{C}}, \overline{\overline{L}}$, and $\overline{\overline{X}}$ for the structure of Fig. 5 as a function of κ. ($C_{22} = C_{11}, C_{12} = C_{21}, L_{22} = L_{11}, L_{12} = L_{21}, X_{22} = X_{11}, X_{12} = X_{21}$,and $\Re(\overline{\overline{X}}) = 0$).

$$+j\begin{pmatrix} 51.37 & -114.82 & -50.80 & -3.69 \\ 373.85 & -5.01 & -115.35 & 28.17 \\ 256.64 & 71.84 & -52.03 & 5.68 \\ 204.56 & -6.49 & -37.76 & 8.79 \end{pmatrix} \text{ps/m} \tag{23}$$

and the $\overline{\overline{Y}}$-matrix is the Hermitian conjugate of the $\overline{\overline{X}}$-matrix. Particularly interesting are the propagation coefficients of the eight modes (four in each direction)

$$\begin{aligned} \beta_{1,+}/k_0 &= 1.5484 \quad \beta_{1,-}/k_0 = 1.5501 \\ \beta_{2,+}/k_0 &= 1.6970 \quad \beta_{2,-}/k_0 = 1.6955 \\ \beta_{3,+}/k_0 &= 1.7998 \quad \beta_{3,-}/k_0 = 1.7989 \\ \beta_{4,+}/k_0 &= 1.8433 \quad \beta_{4,-}/k_0 = 1.8451. \end{aligned} \tag{24}$$

This clearly shows that the structure of Fig. 4 is not bi-directional.

As a third example we consider the more complicated structure of Fig. 5 consisting of two horseshoe-shaped conductors embedded in a three-layered chiral medium surrounded by a cylinder. This structure illustrates the possibility of analyzing closed structures containing layered media. The surrounding cylinder is chosen as ground conductor. Fig. 6 shows the $\overline{\overline{C}}, \overline{\overline{L}}$, and $\overline{\overline{X}}$ matrices for this structure as a function of the chirality parameter κ of the central layer. Due to the symmetry in the structure it is clear that $C_{12} = C_{21}, C_{22} = C_{11}, L_{12} = L_{21}, L_{22} = L_{11}, X_{12} = X_{21}$, and $X_{22} = X_{11}$. On the other hand, since the structure contains only chiral materials, the $\overline{\overline{X}}$ matrix is purely imaginary and the $\overline{\overline{Z}}$ matrix is equal to $-\overline{\overline{X}}$. Note also that $\overline{\overline{X}}$ is different from zero, although the structure is higly symmetric. The reason for this is that the symmetry is a point symmetry in the cross-section and not a line mirror symmetry in the cross-section. If κ is replaced by the Tellegen parameter χ then $\overline{\overline{C}}$ and $\overline{\overline{L}}$ remain unchanged and $\overline{\overline{X}}$ is replaced by $-j\overline{\overline{X}}$, i.e. the new $\overline{\overline{X}}$ becomes real.

V. Conclusion

A method of moments and pointmatching space-domain integral equation technique has been implemented to determine the bitransmission line parameters $\overline{\overline{C}}, \overline{\overline{L}}, \overline{\overline{X}}$, and $\overline{\overline{Z}}$ for general-shaped multiconductor transmission lines embedded in multi-layered bi-isotropic media. The theory has been illustrated by a number of examples showing the generality and accuracy of the method.

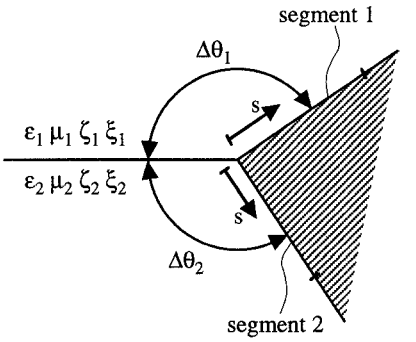

Fig. 7. Edge at the interface between two layers.

VI. Appendix

First we discuss the values of ν_1, ν_2, α_1, and α_2 in (6) for segments at the edges of conductors. For an edge not at a layer interface, i.e. an edge in homogeneous material, nothing changes with respect to the isotropic case of [7]. This means that $\alpha_1 = \alpha_2 = 0$ and that $\nu_1 = \nu_2 = \pi/\Delta\theta$ with $\Delta\theta$ the opening angle of the conductor. For an edge on a layer interface, such as is the case for a microstrip line, things are more complicated. The situation and notations are depicted on Fig. 7. As is shown in [9], ν_1 and ν_2 are the two smallest positive solutions of the following transcendental equation:

$$\begin{aligned} &(\mu_1 S_1 C_2 + \mu_2 S_2 C_1)\left(\frac{\mu_1}{n_1^2} S_1 C_2 + \frac{\mu_2}{n_2^2} S_2 C_1\right) \\ &\quad - \frac{1}{n_1^2 n_2^2}(\mu_2\xi_1 - \mu_1\xi_2)(\mu_2\zeta_1 - \mu_1\zeta_2) S_1^2 S_2^2 = 0 \end{aligned} \tag{25}$$

with $S_i = \sin(\nu\Delta\theta_i)$ and $C_i = \cos(\nu\Delta\theta_i)$ $(i = 1, 2)$. The α_1 and α_2 coefficients for segment 1 in layer 1 are given by

$$\alpha_1 = -\left.\frac{\mu_1 n_2^2 S_1 C_2 + \mu_2 n_1^2 S_2 C_1}{(\mu_2\xi_1 - \mu_1\xi_2) S_1 S_2 n_1^2}\right|_{\nu=\nu_1}$$

$$\bar{\bar{b}} = \begin{pmatrix} \bar{\bar{A}}\begin{pmatrix} D_{11} & D_{12} \\ D_{41} & D_{42} \end{pmatrix} + \begin{pmatrix} D_{21} & D_{22} \\ D_{31} & D_{32} \end{pmatrix} & -\bar{\bar{A}}\begin{pmatrix} U_{11} & U_{12} \\ U_{41} & U_{42} \end{pmatrix} - \begin{pmatrix} U_{21} & U_{22} \\ U_{31} & U_{32} \end{pmatrix} \\ \bar{\bar{A}}\begin{pmatrix} D_{11} & D_{12} \\ D_{41} & D_{42} \end{pmatrix} - \begin{pmatrix} D_{21} & D_{22} \\ D_{31} & D_{32} \end{pmatrix} & -\bar{\bar{A}}\begin{pmatrix} U_{11} & U_{12} \\ U_{41} & U_{42} \end{pmatrix} + \begin{pmatrix} U_{21} & U_{22} \\ U_{31} & U_{32} \end{pmatrix} \end{pmatrix} \tag{30}$$

$$\frac{1}{\alpha_2} = -\left.\frac{\mu_1 n_2^2 S_1 C_2 + \mu_2 n_1^2 S_2 C_1}{(\mu_2\xi_1 - \mu_1\xi_2) S_1 S_2 n_1^2}\right|_{\nu=\nu_2}. \tag{26}$$

The α_1 and α_2 coefficients for segment 2 in layer 2 are found by interchanging the indices 1 and 2 on the right hand sides of (26) and by changing the signs of these expressions.

As a second part of this appendix we give the full expressions for the quantities $\boldsymbol{R}^{d(i)}$ and $\boldsymbol{R}^{u(i)}$ $(i = 1, 2)$ in (16)

$$\boldsymbol{R}^{d(1)} = \frac{1}{\Xi}\begin{pmatrix} -\frac{n_e^2}{\mu_e}c_{13} \\ -\frac{n_e^2}{\mu_e}c_{23} \end{pmatrix} \quad \boldsymbol{R}^{d(2)} = \frac{1}{\Xi}\begin{pmatrix} \frac{n_e^2}{\mu_e}c_{11} \\ \frac{n_e^2}{\mu_e}c_{21} \end{pmatrix}$$
$$\boldsymbol{R}^{u(1)} = \frac{1}{\Xi}\begin{pmatrix} \frac{n_e^2}{\mu_e}c_{31} \\ \frac{n_e^2}{\mu_e}c_{41} \end{pmatrix} \quad \boldsymbol{R}^{u(2)} = \frac{1}{\Xi}\begin{pmatrix} -\frac{n_e^2}{\mu_e}c_{33} \\ -\frac{n_e^2}{\mu_e}c_{43} \end{pmatrix} \tag{27}$$

with Ξ defined as

$$\begin{aligned} \Xi = {} & (b_{13}b_{24} - b_{14}b_{23})(b_{31}b_{42} - b_{32}b_{41}) \\ & + \exp(-2k_x d_e)[(b_{11}b_{24} - b_{14}b_{21})(b_{32}b_{43} - b_{33}b_{42}) \\ & + (b_{13}b_{21} - b_{11}b_{23})(b_{32}b_{44} - b_{34}b_{42}) \\ & + (b_{12}b_{23} - b_{13}b_{22})(b_{31}b_{44} - b_{34}b_{41}) \\ & + (b_{14}b_{22} - b_{12}b_{24})(b_{31}b_{43} - b_{33}b_{41})] \\ & + \exp(-4k_x d_e)(b_{11}b_{22} - b_{12}b_{21})(b_{33}b_{44} - b_{34}b_{43}) \end{aligned} \tag{28}$$

and the elements c_{ij} $(i, j = 1, 2, 3, 4)$ as

$$\begin{aligned} c_{(3-j)(3-k)} = {} & (-1)^{j+k}\{\exp(-2k_x d_e)b_{kj}(b_{33}b_{44} - b_{34}b_{43}) \\ & + [b_{k3}(b_{34}b_{4j} - b_{3j}b_{44}) \\ & + b_{k4}(b_{3j}b_{43} - b_{33}b_{4j})]\} \\ c_{(2+j)(2+k)} = {} & (-1)^{j+k}\{\exp(-2k_x d_e)b_{(5-k)(5-j)} \\ & \cdot (b_{11}b_{22} - b_{12}b_{21}) \\ & + [b_{1(5-j)}(b_{21}b_{(5-k)2} - b_{22}b_{(5-k)1}) \\ & + b_{2(5-j)}(b_{12}b_{(5-k)1} - b_{11}b_{(5-k)2})]\} \\ c_{(3-j)(2+k)} = {} & (-1)^{j+k+1}\{b_{(5-k)j}(b_{13}b_{24} - b_{14}b_{23}) \\ & + \exp(-2k_x d_e)[b_{1j}(b_{23}b_{(5-k)4} - b_{24}b_{(5-k)3}) \\ & + b_{2j}(b_{14}b_{(5-k)3} - b_{13}b_{(5-k)4})]\} \\ c_{(2+j)(3-k)} = {} & (-1)^{j+k+1}\{b_{k(5-j)}(b_{31}b_{42} - b_{41}b_{32}) \\ & + \exp(-2k_x d_e)[b_{3(5-j)}(b_{k2}b_{41} - b_{k1}b_{42}) \\ & + b_{4(5-j)}(b_{k1}b_{32} - b_{k2}b_{31})]\} \\ & j = 1, 2 \quad k = 1, 2 \end{aligned} \tag{29}$$

where b_{ij} $(i, j = 1, 2, 3, 4)$ are the elements of the matrix $\bar{\bar{b}}$ defined as (30), shown at the top of the page, where U_{ij} and D_{ij} $(i = 1, 2, 3, 4$ and $j = 1, 2)$ are, respectively, the elements of $\bar{\bar{U}}_e$ and $\bar{\bar{D}}_e$ defined in (15) and where $\bar{\bar{A}}$ is defined as

$$\bar{\bar{A}} = \begin{pmatrix} k_x\varepsilon_e & -j\xi_e \\ j\zeta_e & \frac{\mu_e}{k_x} \end{pmatrix}. \tag{31}$$

Finally we give the expressions for the $A_{a\rho}(k_x)$, $B_{a\rho}(k_x), C_{a\rho}(k_x)$, and $D_{a\rho}(k_x)$ coefficients in (18)

$$\begin{aligned} \begin{pmatrix} A_{\phi\rho}(k_x) \\ A_{\psi\rho}(k_x) \end{pmatrix} &= \frac{1}{2}\begin{pmatrix} 1 & \frac{\mu_o}{k_x n_o^2} & j\frac{\xi_o}{n_o^2} & 0 \\ j\zeta_o & 0 & 1 & \frac{\mu_o}{k_x} \end{pmatrix}\bar{\bar{U}}_o\boldsymbol{R}^{u(1)} \\ \begin{pmatrix} B_{\phi\rho}(k_x) \\ B_{\psi\rho}(k_x) \end{pmatrix} &= \frac{1}{2}\begin{pmatrix} 1 & \frac{\mu_o}{k_x n_o^2} & j\frac{\xi_o}{n_o^2} & 0 \\ j\zeta_o & 0 & 1 & \frac{\mu_o}{k_x} \end{pmatrix}\bar{\bar{U}}_o\boldsymbol{R}^{u(2)} \\ \begin{pmatrix} C_{\phi\rho}(k_x) \\ C_{\psi\rho}(k_x) \end{pmatrix} &= \frac{1}{2}\begin{pmatrix} 1 & -\frac{\mu_o}{k_x n_o^2} & -j\frac{\xi_o}{n_o^2} & 0 \\ -j\zeta_o & 0 & 1 & -\frac{\mu_o}{k_x} \end{pmatrix} \\ &\quad \cdot \bar{\bar{U}}_o\boldsymbol{R}^{u(1)} \\ \begin{pmatrix} D_{\phi\rho}(k_x) \\ D_{\psi\rho}(k_x) \end{pmatrix} &= \frac{1}{2}\begin{pmatrix} 1 & -\frac{\mu_o}{k_x n_o^2} & -j\frac{\xi_o}{n_o^2} & 0 \\ -j\zeta_o & 0 & 1 & -\frac{\mu_o}{k_x} \end{pmatrix} \\ &\quad \cdot \bar{\bar{U}}_o\boldsymbol{R}^{u(2)}. \end{aligned} \tag{32}$$

REFERENCES

[1] F. Olyslager, E. Laermans, and D. De Zutter, "Rigorous quasi-TEM analysis of multiconductor transmission lines in bi-isotropic media—Part I: Theoretical analysis for general inhomogeneous media and generalization to bianisotropic media," *IEEE Trans. Microwave Theory Tech.*, vol. 43, no. 7, pp. 1409–1415, July 1995.

[2] F. Olyslager and D. De Zutter, "Rigourous full-wave analysis of electric and dielectric waveguides embedded in a multilayered bianisotropic medium," *Radio Sci.*, vol. 28, pp. 937–946, Sept./Oct. 1993.

[3] C. M. Krowne, "Vector varational and weigthed residual finite element procedures for highly anisotropic media," *IEEE Trans. Antennas Propagat.*, vol. 42, no. 5, pp. 642–650, May 1994.

[4] C. Wei, R. F. Harrington, J. R. Mautz, and T. K. Sarkar, "Multiconductor transmission lines in multilayered dielectric media," *IEEE Trans. Microwave Theory Tech.*, vol. MTT-32, no. 4, pp. 439–450, Apr. 1984.

[5] R. F. Harrington and C. Wei, "Losses on multiconductor transmission lines in multilayered dielectric media," *IEEE Trans. Microwave Theory Tech.*, vol. MTT-32, no. 7, pp. 705–710, July 1984.

[6] W. Delbare and D. De Zutter, "Space-domain Green's function approach to the capacitance calculation of multiconductor lines in multilayered dielectrics with improved surface charge modelling," *IEEE Trans. Microwave Theory Tech.*, vol. MTT-37, no. 10, pp. 1562–1568, Oct. 1989.

[7] F. Olyslager, N. Faché, and D. De Zutter, "New fast and accurate line parameter calculation of multiconductor transmission lines in multilay-

ered media," *IEEE Trans. Microwave Theory Tech.*, vol. 39, no. 6, pp. 901–909, June 1991.

[8] M. Horno, F. L. Mesa, F. Medina, and R. Marques, "Quasi-TEM analysis of multilayered, multiconductor coplanar structures with dielectric and magnetic anisotropy including substrate losses," *IEEE Trans. Microwave Theory Tech.*, vol. 38, no. 8, pp. 1059–1068, Aug. 1990.

[9] F. Olyslager, "The behavior of electromagnetic fields at edges in bi-isotropic and bi-anisotropic materials," *IEEE Trans. Antennas Propagat.*, vol. 42, no. 10, pp. 1392–1397, Oct. 1994.

[10] P. K. Koivisto and J. C.-E. Sten, "Quasi-static image method applied to bi-isotropic microstrip geometry," accepted for publication in *IEEE Trans. Microwave Theory Tech.*, vol. 43, no. 1, pp. 169–175, Jan. 1995.

Frank Olyslager (S'90–M'94), for a photograph and biography, see this issue, p. 1415.

Eric Laermans, for a photograph and biography, see this issue, p. 1415.

Daniël De Zutter (M'92), for a photograph and biography, see this issue, p. 1415.